PHOTONICS Research

Flat gain over arbitrary orbital angular momentum modes in Brillouin amplification

HONGWEI LI,[1,2] BO ZHAO,[1,2] LIWEI JIN,[1,2] DONGMEI WANG,[1,2] AND WEI GAO[1,2,*]

[1]Heilongjiang Provincial Key Laboratory of Quantum Manipulation & Control, Harbin University of Science and Technology, Harbin 150080, China
[2]Department of Physics, School of Science, Harbin University of Science and Technology, Harbin 150080, China
*Corresponding author: wei_g@163.com

Received 7 March 2019; revised 1 May 2019; accepted 6 May 2019; posted 9 May 2019 (Doc. ID 361886); published 11 June 2019

Controlled obtaining of orbital angular momentum (OAM) modes of light at high power over arbitrary orders has important implications for future classical and quantum systems. Appreciable optical amplification has recently been observed for low-order or specific-order OAM modes. However, large amplification of high-order OAM modes still remains challenging. Here we report on flat-gain amplification of arbitrary OAM modes via Brillouin interactions and demonstrate that the OAM modes with various orders can be efficiently and relatively uniformly amplified by imaging the wave source of OAM mode propagation in a nonlinear medium. Meanwhile, the propagation properties of beams carrying OAM with arbitrary modes are high-fidelity maintained. This work provides a practicable way to flatten the mode gain and represents a crucial necessity to realize OAM mode filters with controllable mode gain bandwidth.

https://doi.org/10.1364/PRJ.7.000748

1. INTRODUCTION

Since Allen *et al.* pointed out that a light with a helical phase factor $\exp(il\varphi)$ carries orbital angular momentum (OAM) of $l\hbar$ per photon, where φ is the azimuthal angle and l is the order of an OAM mode. The light beams carrying OAM have attracted immense interest for their unique features of inherently infinite dimensionality and mechanical properties [1,2], and have exhibited potential applications in optical micromanipulation [3], high-capacity optical communications and mode-division multiplexing [4–6], enhanced imaging [7,8], high-dimension quantum information [9–11], fundamental or scientific research for optics [12–19], and quantum theory [20]. In addition, there has also been a recent surge for generating beams carrying OAM with high power and fidelity for future classical and quantum systems [21–28]. These techniques mainly focus on amplification of low-order modes or specific modes depending on designed few-mode fibers. As a next stage, uniform and selective amplification of OAM modes with arbitrary orders is reasonable and imperative to satisfy application requirements of high-power OAM modes and mode filters.

We have demonstrated efficient amplification with high fidelity, high gain, and low noise for the OAM mode of $l = 1$ and cylindrical vector pulses in a Brillouin-based optical amplifier [29,30]. The Brillouin amplification, a kind of third-order nonlinear process via light–acoustic interaction [31], has been a subject of interest because of its rapid development in silicon-based photonics [32–36], laser beam combination [37], optical fiber sensing and filtering [38–40], coherent transmission of optical frequencies [41], and microscopy [42,43]. Prabhakar *et al.* have demonstrated the phase conjugation in OAM fiber modes via stimulated Brillouin scattering (SBS). They observed the phase conjugate modes with $l = 9$, 10, 11, and 12 have similar SBS powers or gain for the pump mode with $l = 11$, whereas the gain of other modes decreased dramatically [44]. We have recently explored OAM mode-division filtering to remove SBS noise, and observed that the high-order modes can be employed on-demand to achieve a better signal–noise separation, however, with a lower Brillouin gain [45]. In this work, we aim to achieve flat gain over arbitrary orders in a Brillouin amplifier (BA). We first investigate the dependence of OAM mode gain on its order. The gain decreasing with the orders is ascribed to a poor overlap of interaction modes. To address this issue, we then present a method for flattening the mode gain spectrum as a function of the orders. By imaging the order-independent wave sources of propagation of OAM modes in a nonlinear medium, we eliminate the dependence of the overlap on the order. Moreover, the propagation properties of amplified OAM modes are the same as those of input OAM modes. This technique can also be applied in other optical amplifications or nonlinear interactions involving OAM mode overlap.

2. THEORETICAL ANALYSIS

In the Brillouin amplification, the intensity equation satisfied by the Stokes field can be given by

$$\frac{dI_S}{dz} = -g_0 I_S I_P, \tag{1}$$

where g_0 is the maximum Brillouin gain coefficient, z is the propagating distance, and I_P and I_S are the intensity of the pump and Stokes beam, respectively. Since we are now considering the different transverse intensity distribution between the donut-profile Stokes and Gaussian-profile pump beam, it is useful to consider the total power in each beam, defined by [46]

$$P_P = \iint I_P dxdy, \qquad P_S = \iint I_S dxdy, \tag{2}$$

where the integrals are to be carried out over an area large enough to include essentially all of the power contained in each beam. Equation (1) can then be described in the form

$$\frac{dP_S}{dz} = -g_0 \frac{P_P P_S}{\sigma} \eta, \tag{3}$$

where $\sigma = \iint dxdy$ is the integral area and where

$$\eta = \frac{\left| \iint E_P(x,y,z) E_S(x,y,z) dxdy \right|^2}{\iint |E_P(x,y,z)|^2 dxdy \iint |E_S(x,y,z)|^2 dxdy} \tag{4}$$

represents the spatial cross-correlation function of the pump and Stokes intensity distributions (i.e., intensity overlap integral), and $E_P(x,y,z)$ and $E_S(x,y,z)$ are the amplitudes of pump and Stokes beam, respectively. We reported the observation of reversible OAM transfer in photon–phonon conversion, and proposed the corresponding OAM selection rules via Brillouin amplification in a liquid medium [14]. Compared to the multiphonon OAM modes in special fiber [38,44], in liquid medium, the phonon OAM mode excited by Brillouin interaction has the same order as the Stokes beam in the case of the pump with Gaussian mode. Therefore, we only consider the optical overlap integral in the theoretical model. We consider satisfying the phase-matching condition and ignore the transverse variation of the pump and Stokes fields. By solving Eq. (3), we can obtain

$$P_S = P_{S0} \exp\left[g_0 \eta \frac{P_P}{\sigma}(L-z)\right] = P_{S0} \exp\left[g_{\text{eff}} \frac{P_P}{\sigma}(L-z)\right], \tag{5}$$

where P_{S0} is the input Stokes beam power and $g_{\text{eff}} = g_0 \eta$ is the effective gain coefficient, depending on the overlap of the interaction beams. The amplified beam intensity grows exponentially with distance as it propagates in the $-z$ direction starting from an initial value at $z = L$, and L is the total interaction length.

The OAM mode can be generated by the addition of a helical phase factor $\exp(il\varphi)$ to the Gaussian-illuminating beam through a spiral phase plate (SPP). The light field at the rear plane of the SPP can be regarded as the wave source of OAM mode propagation ($z' = 0$) and is written as

$$E_0(x_0, y_0, 0) = \sqrt{\frac{2}{\pi}} \frac{1}{\omega_0} \exp\left(-\frac{x_0^2 + y_0^2}{\omega_0^2}\right) \exp(-il\varphi_0), \tag{6}$$

where ω_0 is the illuminating Gaussian beam waist, and $\varphi_0 = \arctan(y_0/x_0)$. It is obvious that the wave sources have the Gaussian profiles for arbitrary-order OAM modes. After propagating away from the SPP, the light field can be obtained from the Collins diffraction integral equation [47,48]

$$\begin{aligned} E(x,y,z') = {} & \frac{i^{l+1}}{\lambda z' \omega_0} \sqrt{\frac{2}{\pi} \frac{1}{2\varepsilon}} \left(\frac{b^2}{\varepsilon}\right)^{\frac{l}{2}} \exp(-ikz') \\ & \times \exp\left[-\frac{ik}{2z'}(x^2+y^2)\right] \cdot \exp(-il\varphi) \frac{\Gamma\left(\frac{l}{2}+1\right)}{\Gamma(l+1)} \\ & \times F\left(\frac{l}{2}+1, l+1, -\frac{b^2}{\varepsilon}\right), \end{aligned} \tag{7}$$

where z' is the axial distance from the beam waist, $k = 2\pi/\lambda$ is the wavenumber, $\Gamma(\xi)$ is the gamma function, $F(\alpha, \gamma, \beta)$ is a confluent hypergeometric function, and the parameters ε and b can be defined as

$$\varepsilon = \frac{1}{\omega_0^2} + \frac{ik}{2z'}, \qquad b = \frac{k\sqrt{x^2+y^2}}{2z'}. \tag{8}$$

Figures 1(a1)–1(a5) show the beam evolution behavior upon propagation for $l = 1$; in contrast, we can see the beam intensity distributions at the same propagating distance of high-order OAM modes (e.g., $l = 10$), shown in Figs. 1(b1)–1(b5). The radius of the initial beam waist is set to 0.65 mm. When a helical phase factor $\exp(il\varphi)$ is suddenly imprinted on an ordinary Gaussian beam, a phase singularity with multirings in the outer region of the beam appears and starts to grow radially upon propagation by the effect of diffraction. The beam with the higher order OAM mode has stronger diffraction effects, and so the phase singularities and beam sizes change more rapidly as the propagation distance increases. Additionally, we can see from Figs. 1(a1) and 1(b1) that the wave sources of OAM modes have Gaussian-like intensity distribution as described by Eq. (6).

Figures 1(c1)–1(c5) show the intensity distribution of Stokes beams carrying OAM modes of $l = 0, 2, 4, 6, 8$, respectively, at the propagating distance of 40 cm. It can be seen that the donut shape gradually enlarges with the order of OAM modes. As a result, intensity correlation coefficient η will be decreased versus orders. If the nonlinear interaction occurs between the Gaussian-like wave source of the OAM-carrying

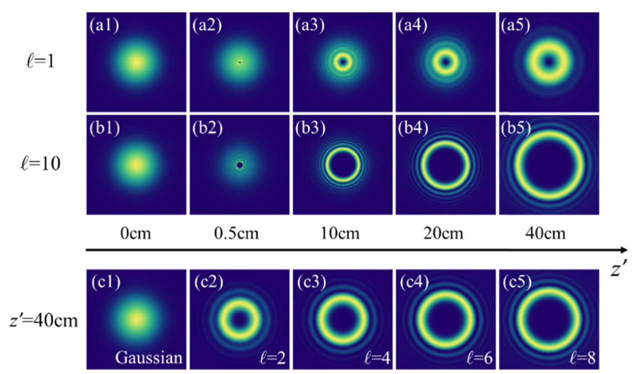

Fig. 1. Simulation results. The propagation evolution in free space of the vortex beam with $l = 1$ (a1)–(a5) and $l = 10$ (b1)–(b5), respectively. The intensity distributions of the (c1) Gaussian-shaped pump beam and (c2)–(c5) OAM-carrying Stokes signal beams with different orders at the propagating distance of 40 cm, respectively.

beam and Gaussian-profile pump beam, η will be constantly equal to 1, and hence g_{eff} should be independent of OAM mode orders. According to theoretical analyses above, we present a method to obtain flat gain over arbitrary OAM mode by using wave sources as the main interaction area. This scheme can be implemented by imaging the wave source into the nonlinear medium using the 4f imaging system. The ABCD matrix of the 4f imaging system with two lenses can be described by

$$\begin{bmatrix} A & B \\ C & D \end{bmatrix} = \begin{bmatrix} -\frac{f_2}{f_1} & 0 \\ 0 & -\frac{f_1}{f_2} \end{bmatrix}, \tag{9}$$

where f_1 and f_2 represent the focal length of the two lenses, respectively. The light field in imaging plane related to the object plane can be written as [48]

$$E'(x_i, y_i, d) = \frac{1}{A} \exp(ikd) \exp\left[\frac{ikC}{A}(x_i^2 + y_i^2)\right] E_0\left(\frac{x_i}{A}, \frac{y_i}{A}, 0\right), \tag{10}$$

where x_i and y_i are the coordinates in the image plane, and d is the distance between object plane and image plane. Through the 4f imaging system, the output field is a replica of the wave source of OAM modes at the object plane without any extra phase terms and can be given by

$$I'(x_i, y_i, d) = \frac{2}{\pi\omega_0^2 A^2} \exp\left\{-2\left[\left(\frac{x_0}{A}\right)^2 + \left(\frac{y_0}{A}\right)^2\right] \Big/ \omega_0^2\right\}. \tag{11}$$

It is worth noting that the intensity profiles at the image plane will be Gaussian-like profiles for input OAM modes with different orders. This is the key to the realization of the flat gain of OAM modes. The propagation rule after the 4f imaging system can be obtained from the Collins diffraction integral equation. The ABCD matrix of the propagation of light field through the two-lens system with $f_1 = f_2$ can be expressed as

$$\begin{bmatrix} A & B \\ C & D \end{bmatrix} = \begin{bmatrix} -1 & d' \\ 0 & -1 \end{bmatrix}, \tag{12}$$

where d' is the propagation distance of the beam away from the image plane. We then find that, through the lens system, the light field form is the same as Eq. (7), and the parameters ε and b can then be turned into

$$\varepsilon = \frac{1}{\omega_0^2} - \frac{ik}{2d'}, \qquad b = \frac{k\sqrt{x_0^2 + y_0^2}}{2d'}. \tag{13}$$

We can use the results given in Eqs. (13) and (7) to provide theoretical analysis of the propagation behavior near the image plane. Figures 2(a)–2(c) show the simulation results. It can be seen that the intensity distribution at the image plane ($d' = 0$ in Fig. 2) is consistent with a Gaussian-like profile. The high-order OAM modes have poor ability to maintain Gaussian-like intensity distribution when it is far from the image plane. If the Brillouin gain medium is short enough, we can achieve efficient amplification of OAM modes independent of the order. It should be noted that the gain depends on the power density of two beams. Hence, a higher gain can be obtained by reducing the focal length of the lens. Figures 2(d1)–2(d9) show the intensity distribution for OAM modes of $l = 10$ when $f_1 = 10$ cm and $f_2 = 5$ cm. The beam radius near the image plane will be halved (i.e., $A\omega_0$).

3. EXPERIMENTAL RESULTS AND DISSCUSSION

The experimental configuration is illustrated in Fig. 3. On the left side of the BA cell, the pump beam has a Gaussian-shape intensity profile. The central wavelength of the Gaussian-pulse pump beam is 532 nm, with the pulse width 7.8 ns. A combination of a half-wave plate (HWP) and polarizing beam splitter (PBS1) is used to adjust the pump power. On the other side, a 6.9 ns Gaussian-pulse signal beam with a Stokes frequency shift is used as the signal beam. By passing through an SPP (RPC Photonics, VPP–m1064), the beam carries OAM. In order to image the field of the signal beam just at the output facet of the SPP to the center of the BA cell, we employ a 4f imaging system with two lenses. Both lenses have a focal length of 10 cm. The detailed dimensions of the image system in our experiments show that the central position of the BA cell is 15 cm away from L1 and the distance between SPP and L2 is 5 cm. After passing through the quarter-wave plate (QWP1

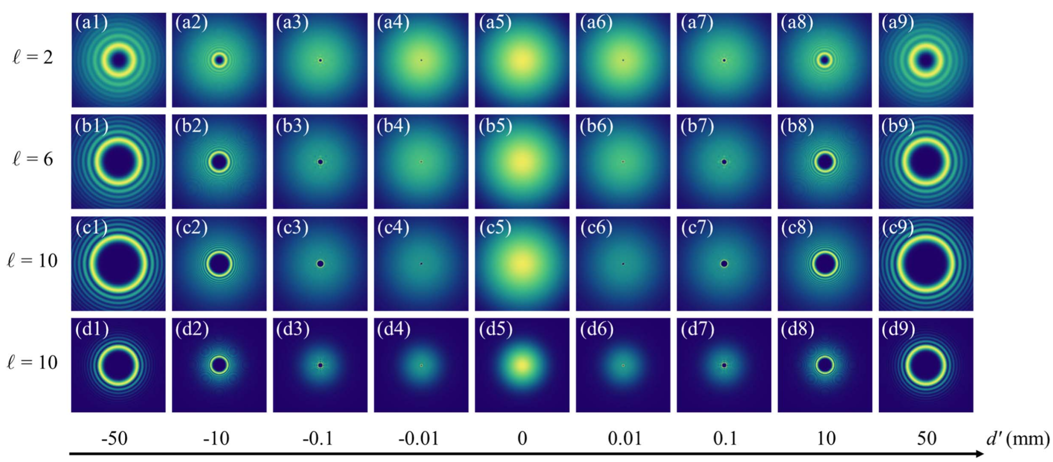

Fig. 2. Simulation results for the propagation behavior of Stokes beams with $l = 2$, 6, and 10 near the image plane through (a)–(c) two lenses with $f_1 = f_2 = 10$ cm, respectively, and (d1)–(d9) two lenses with $f_1 = 10$ cm and $f_2 = 5$ cm, respectively, for $l = 10$.

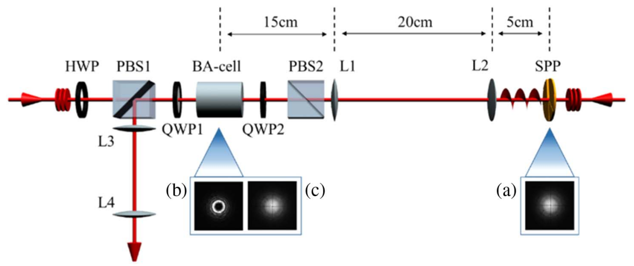

Fig. 3. Experimental setup. HWP, half-wave plate; PBS1 and PBS2, polarized beam splitter; QWP1 and QWP2, quarter-wave plate; BA-cell, Brillouin amplifier cell; L1–L4, lens. (a) The intensity distribution of the wave source of the OAM mode. The intensity distribution of the OAM mode at the center of BA-cell (b) without and (c) with utilizing the 4f imaging system.

and QWP2), the beams with left and right circular polarizations are generated. These two beams interact in a 10-cm-long BA cell contained CS_2, and the amplified signal outputs from left side of the BA cell are reflected from the PBS1. Both ends of the BA cell have high-transmission coating ($T > 95\%$) at 532 nm, and the diameter of the BA cell is 25.4 mm. In the output path, we employ another 4f imaging system including L3 and L4 for secondary imprinting of the amplified beam on a CCD. We use a CCD and an energy meter to record the intensity distribution and energy of the output beam.

When a Gaussian beam passes through the SPP, a spiral wavefront character is imprinted on the incident wave, where a phase singularity at the core of the beam is generated. The wave source of the OAM-carrying beam has a Gaussian-like profile, as shown in Fig. 3(a). Then the beam reaches the center of the BA cell with a propagating distance of 40 cm in free space. We can see that the beam evolves into a donut-shaped beam with multirings, shown in Fig. 3(b). If we employ a 4f imaging system, the Gaussian-like wave source of the OAM mode is located in the center of nonlinear medium, as shown in Fig. 3(c).

In experiment, the powers of all the beams are below the threshold of SBS to avoid self-SBS noise. Figure 4(a) shows the amplified Gaussian-profile Stokes beam. Figures 4(b1)–4(b4) show the intensity profiles of the amplified beam without utilizing the 4f imaging system, where the orders are set to 2, 6, 8, and 10, and the energy of the pump and signal beam is set to 1 mJ and 10 nJ, respectively. We can see that the area and divergence of the amplified OAM Stokes beams increase with the orders at the same propagating distance. As a result, the gain of input OAM modes decreases rapidly with the order, as shown by red circle dots in Fig. 4(e). Experimental data are in good accordance with the simulation results based on Eq. (5). The blue curve and triangle dots in Fig. 4 show the dependence of the OAM mode gain on the order using the 4f imaging system. It should be noted that the mode gain spectrum upon the order is flattened by imaging the wave source into the nonlinear interaction area. The reason for the slight decrease for high-order mode gain is imperfect overlap between the OAM modes at two ends of the BA cell and Gaussian pump beam. We can address this problem by reducing the interaction length and increasing the pump power.

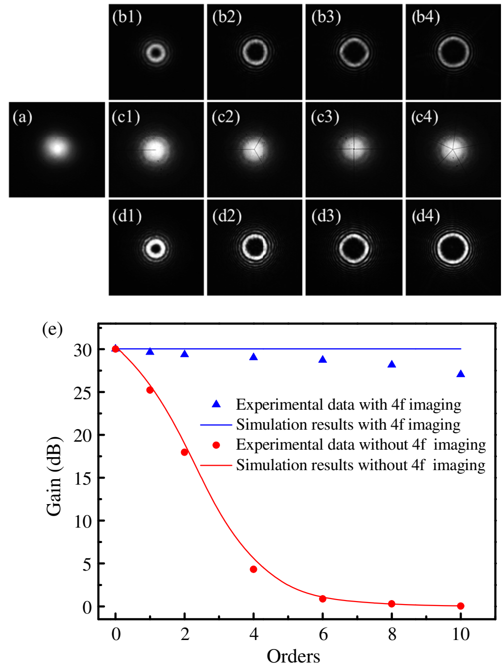

Fig. 4. Experimental results. (a) Amplified Gaussian-profile beam. (b1)–(b4) The intensity distribution of output OAM beams without the 4f imaging system. Utilizing the 4f imaging system, the intensity profiles of the amplified OAM beam at (c1)–(c4) the secondary image plane and (d1)–(d4) the propagating distance of 40 cm, where the orders are set to 2, 6, 8, and 10, respectively. (e) Simulation curves and experimental results of the mode gain versus its orders.

Figures 4(c1)–4(c4) show the observed intensity profiles of the amplified Stokes beams of $l = 2$, 6, 8, and 10 at the imaging plane of wave source, respectively. Then we move the CCD backward. Figures 4(d1)–4(d4) show the intensity distribution of amplified OAM modes after the propagating distance of 40 cm for $l = 2$, 6, 8, and 10, respectively. Compared to Figs. 4(b1)–4(b4), the propagation properties of amplified OAM modes are the same as those without utilizing the 4f imaging system. That is, the 4f system has no impact on the propagation of OAM modes, which are high-fidelity maintained.

Figure 5 shows the dependence of the gain for the OAM mode of $l = 10$ on pump energy by utilizing the 4f imaging system. Like the general Brillouin amplification process, the

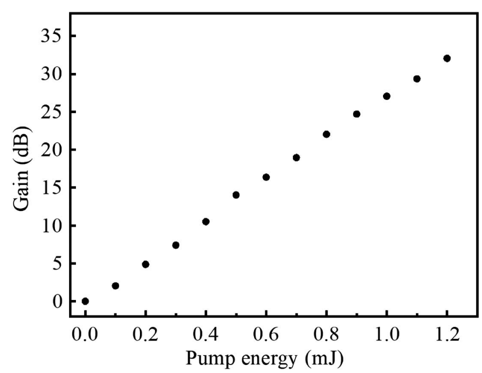

Fig. 5. Gain versus the pump energies for the OAM mode of $l = 10$.

gain increases almost exponentially under the pump nondepletion condition. We obtain a gain as high as ∼32 dB at the maximal limitation of pump energy of 1.2 mJ. We can easily enhance Brillouin gain by increasing the pump energy, as shown in Ref. [29].

4. CONCLUSION

In summary, we have first investigated the dependence of an OAM mode gain spectrum on its order via Brillouin interaction. By utilizing a 4f imaging system, the order-independent wave sources of OAM modes are imaged in a nonlinear medium. Based on this scheme, we eliminate the dependence of the overlap on the order between photon–photon interaction and obtain a flat gain over arbitrary OAM modes in Brillouin amplification. The proof-of-principle demonstration reveals the potential application in Brillouin beam combination systems of arbitrary OAM modes or an SBS noise suppression scheme. Furthermore, this technique provides a practicable way toward relatively uniform and selective-amplification OAM modes, including high-dimensional superposition of multiple OAM modes and realization of OAM mode filters in a mode-division multiplexing system, and it can also be applied in other optical amplifications or nonlinear interactions involving OAM mode overlap.

Funding. National Natural Science Foundation of China (NSFC) (11574065, 61378003).

REFERENCES

1. L. Allen, M. W. Beijersbergen, R. J. C. Spreeuw, and J. P. Woerdman, “Orbital angular momentum of light and the transformation of Laguerre-Gaussian laser modes,” Phys. Rev. A **45**, 8185–8189 (1992).
2. M. J. Padgett, “Orbital angular momentum 25 years on,” Opt. Express **25**, 11265–11274 (2017).
3. M. Padgett and R. Bowman, “Tweezers with a twist,” Nat. Photonics **5**, 343–348 (2011).
4. J. Wang, J. Y. Yang, I. M. Fazal, N. Ahmed, Y. Yan, H. Huang, Y. Ren, Y. Yue, S. Dolinar, and M. Tur, “Terabit free-space data transmission employing orbital angular momentum multiplexing,” Nat. Photonics **6**, 488–496 (2012).
5. P. Chen, L. L. Ma, W. Duan, J. Chen, S. J. Ge, Z. H. Zhu, M. J. Tang, R. Xu, W. Gao, T. Li, W. Hu, and Y. Q. Lu, “Digitalizing self-assembled chiral superstructures for optical vortex processing,” Adv. Mater. **30**, 1705865 (2018).
6. P. Gregg, P. Kristensen, and S. Ramachandran, “Conservation of orbital angular momentum in air-core optical fibers,” Optica **2**, 267–270 (2015).
7. G. Foo, D. M. Palacios, and G. A. Swartzlander, “Optical vortex coronagraph,” Opt. Lett. **30**, 3308–3310 (2005).
8. M. Ritschmarte, “Orbital angular momentum light in microscopy,” Philos. Trans. R. Soc. A **375**, 20150437 (2017).
9. A. Mair, A. Vaziri, G. Weihs, and A. Zeilinger, “Entanglement of the orbital angular momentum states of photons,” Nature **412**, 313–316 (2001).
10. D. S. Ding, W. Zhang, S. Shi, Z. Y. Zhou, Y. Li, B. S. Shi, and G. C. Guo, “High-dimensional entanglement between distant atomic ensemble memories,” Light Sci. Appl. **5**, e16157 (2014).
11. M. Erhard, R. Fickler, M. Krenn, and A. Zeilinger, “Twisted photons: new quantum perspectives in high dimensions,” Light Sci. Appl. **7**, 17146 (2018).
12. A. Aadhi, G. K. Samanta, S. C. Kumar, and M. E. Zadeh, “Controlled switching of orbital angular momentum in an optical parametric oscillator,” Optica **4**, 349–355 (2017).
13. D. Gauthier, P. R. Ribič, G. Adhikary, A. Camper, C. Chappuis, R. Cucini, L. F. Dimauro, G. Dovillaire, F. Frassetto, and R. Géneaux, “Tunable orbital angular momentum in high-harmonic generation,” Nat. Commun. **8**, 14971 (2017).
14. Z. Zhu, C. Mu, H. Li, and W. Gao, “Reversible orbital angular momentum photon–phonon conversion,” Optica **3**, 212–217 (2016).
15. F. Bouchard, J. Harris, H. Mand, R. W. Boyd, and E. Karimi, “Observation of subluminal twisted light in vacuum,” Optica **3**, 351–354 (2016).
16. S. Liu, S. Qi, Y. Zhang, P. Li, D. Wu, L. Han, and J. Zhao, “Highly efficient generation of arbitrary vector beams with tunable polarization, phase, and amplitude,” Photon. Res. **6**, 228–233 (2018).
17. R. Xu, P. Chen, J. Tang, W. Duan, S.-J. Ge, L.-L. Ma, R.-X. Wu, W. Hu, and Y.-Q. Lu, “Perfect higher-order Poincaré sphere beams from digitalized geometric phases,” Phys. Rev. Appl. **10**, 034061 (2018).
18. Y. Li, Z. Y. Zhou, S. L. Liu, S. K. Liu, C. Yang, Z. H. Xu, Y. H. Li, and B. S. Shi, “Frequency doubling of twisted light independent of integer topological charge,” OSA Continuum **2**, 470–477 (2019).
19. J. Vieira, R. M. G. M. Trines, E. P. Alves, R. A. Fonseca, J. T. Mendonca, R. Bingham, P. Norreys, and L. O. Silva, “High orbital angular momentum harmonic generation,” Phys. Rev. Lett. **117**, 265001 (2016).
20. Z. Y. Zhou, Z. H. Zhu, S. L. Liu, Y. H. Li, S. Shi, D. S. Ding, L. X. Chen, W. Gao, G. C. Guo, and B. S. Shi, “Quantum twisted double-slits experiments: confirming wavefunctions’ physical reality,” Sci. Bull. **62**, 1185–1192 (2017).
21. J. Vieira, R. M. G. M. Trines, E. P. Alves, R. A. Fonseca, J. T. Mendonça, R. Bingham, P. Norreys, and L. O. Silva, “Amplification and generation of ultra-intense twisted laser pulses via stimulated Raman scattering,” Nat. Commun. **7**, 10371 (2016).
22. D. J. Kim, J. W. Kim, and W. A. Clarkson, “High-power master-oscillator power-amplifier with optical vortex output,” Appl. Phys. B **117**, 459–464 (2014).
23. Y. Tanaka, M. Okida, K. Miyamoto, and T. Omatsu, “High power picosecond vortex laser based on a large-mode-area fiber amplifier,” Opt. Express **17**, 14362–14366 (2009).
24. K. Mio, H. Tetsuya, O. Masahito, M. Katsuhiko, and O. Takashige, “Nanosecond vortex laser pulses with millijoule pulse energies from a Yb-doped double-clad fiber power amplifier,” Opt. Express **19**, 14420–14425 (2011).
25. G. C. Borba, S. Barreiro, L. Pruvost, D. Felinto, and J. W. Tabosa, “Narrow band amplification of light carrying orbital angular momentum,” Opt. Express **24**, 10078–10086 (2016).
26. S. Zhu, S. Pidishety, Y. Feng, S. Hong, J. Demas, R. Sidharthan, S. Yoo, S. Ramachandran, B. Srinivasan, and J. Nilsson, “Multimode-pumped Raman amplification of a higher order mode in a large mode area fiber,” Opt. Express **26**, 23295–23304 (2018).
27. E. G. Johnson, K. Miller, R. Shori, W. Li, Y. Li, and Z. Zhang, “Concentric vortex beam amplification: experiment and simulation,” Opt. Express **24**, 1658–1667 (2016).
28. X. Heng, J. Gan, Z. Zhang, Q. Qian, and Z. Yang, “Amplification of orbital angular momentum modes in an erbium-doped solid-core photonic bandgap fiber,” Opt. Commun. **433**, 132–136 (2019).
29. W. Gao, C. Y. Mu, H. W. Li, Y. Q. Yang, and Z. H. Zhu, “Parametric amplification of orbital angular momentum beams based on light-acoustic interaction,” Appl. Phys. Lett. **107**, 299–313 (2015).
30. Z. H. Zhu, P. Chen, L. W. Sheng, Y. L. Wang, W. Hu, Y. Q. Lu, and W. Gao, “Generation of strong cylindrical vector pulses via stimulated Brillouin amplification,” Appl. Phys. Lett. **110**, 141104 (2017).
31. C. Guodong, Z. Ruiwen, S. Junqiang, X. Heng, G. Ya, F. Danqi, and X. Huang, “Mode conversion based on forward stimulated Brillouin scattering in a hybrid phononic-photonic waveguide,” Opt. Express **22**, 32060–32070 (2014).
32. B. Lutherdavies, B. J. Eggleton, B. Morrison, D. Marpaung, D. Y. Choi, M. Pagani, R. Pant, and S. J. Madden, “Low-power, chip-based stimulated Brillouin scattering microwave photonic filter with ultrahigh selectivity,” Optica **2**, 76–83 (2015).
33. H. Jiang, D. Marpaung, M. Pagani, K. Vu, D. Y. Choi, S. J. Madden, L. Yan, and B. J. Eggleton, “Wide-range, high-precision multiple

microwave frequency measurement using a chip-based photonic Brillouin filter," Optica **3**, 30–34 (2016).
34. E. A. Kittlaus, H. Shin, and P. T. Rakich, "Large Brillouin amplification in silicon," Nat. Photonics **10**, 463–467 (2016).
35. E. A. Kittlaus, N. T. Otterstrom, P. Kharel, S. Gertler, and P. T. Rakich, "Non-reciprocal interband Brillouin modulation," Nat. Photonics **12**, 613–619 (2018).
36. S. Gundavarapu, G. M. Brodnik, M. Puckett, T. Huffman, D. Bose, R. Behunin, J. Wu, T. Qiu, C. Pinho, N. Chauhan, J. Nohava, P. T. Rakich, K. D. Nelson, M. Salit, and D. J. Blumenthal, "Sub-hertz fundamental linewidth photonic integrated Brillouin laser," Nat. Photonics **13**, 60–67 (2019).
37. C. Cui, Y. Wang, Z. Lu, H. Yuan, Y. Wang, Y. Chen, Q. Wang, Z. Bai, and R. P. Mildren, "Demonstration of 2.5 J, 10 Hz, nanosecond laser beam combination system based on non-collinear Brillouin amplification," Opt. Express **26**, 32717–32727 (2018).
38. Y. P. Xu, M. Q. Ren, Y. Lu, P. Lu, P. Lu, X. Y. Bao, L. X. Wang, Y. Messaddeq, and S. Larochelle, "Multi-parameter sensor based on stimulated Brillouin scattering in inverse-parabolic graded-index fiber," Opt. Lett. **41**, 1138–1141 (2016).
39. G. Yang, X. Fan, B. Wang, and Z. He, "Enhancing strain dynamic range of slope-assisted BOTDA by manipulating Brillouin gain spectrum shape," Opt. Express **26**, 32599–32607 (2018).
40. W. Wei, L. Yi, Y. Jaouën, and W. Hu, "Arbitrary-shaped Brillouin microwave photonic filter by manipulating a directly modulated pump," Opt. Lett. **42**, 4083–4086 (2017).
41. O. Terra, G. Grosche, and H. Schnatz, "Brillouin amplification in phase coherent transfer of optical frequencies over 480 km fiber," Opt. Express **18**, 16102–16111 (2010).
42. Z. Meng, A. J. Traverso, C. W. Ballmann, M. A. Troyanova-Wood, and V. V. Yakovlev, "Seeing cells in a new light: a renaissance of Brillouin spectroscopy," Adv. Opt. Photon. **8**, 300–327 (2016).
43. C. W. Ballmann, Z. Meng, A. J. Traverso, M. O. Scully, and V. V. Yakovlev, "Impulsive Brillouin microscopy," Optica **4**, 124–128 (2017).
44. G. Prabhakar, X. Liu, J. Demas, P. Gregg, and S. Ramachandran, "Phase conjugation in OAM fiber modes via stimulated Brillouin scattering," in *Conference on Lasers and Electro-Optics*, OSA Technical Digest (online) (2018), paper FTh1M.4.
45. Z. H. Zhu, L. W. Sheng, Z. W. Lv, W. M. He, and W. Gao, "Orbital angular momentum mode division filtering for photon-phonon coupling," Sci. Rep. **7**, 40526 (2017).
46. R. W. Boyd, *Nonlinear Optics* (Academic, 2008), pp. 440–452.
47. S. A. Collins, "Lens-system diffraction integral written in terms of matrix optics," J. Opt. Soc. Am. A **60**, 1168–1177 (1970).
48. B. D. Lv, *Laser Optics* (Higher Education, 2003), pp. 11–14.